DOI: 10.1007/s12541-010-0060-x

Development of the End-effector Measurement System for a 6-axis Welding Robot

Keyhwan Kim[1], Sungcheul Lee[2], Kyoubum Kim[1], Kyu-yeul Lee[3], Seungjin Heo[4], Kihong Park[4], Jay-il Jeong[4,#] and Jongwon Kim[1]

1 School of Mechanical and Aerospace Engineering, Seoul National University, Seoul, South Korea, 151-742
2 Korean Institute of Machinery and Materials, Daejeon, South Korea, 305-343
3 Department of Naval Architecture and Ocean Engineering, Seoul National University, Seoul, South Korea, 151-742
4 School of Mechanical and Automotive Engineering, Kookmin University, Seoul, South Korea, 136-702
Corresponding Author / E-mail: jayjeong@kookmin.ac.kr, TEL: +82-2-910-4419, FAX: +82-2-910-4419

KEYWORDS: Measurement system, End effector, Gain tuning, Welding robot

We develop a new measurement system which can measure position and orientation of the end-effector of a six-axis welding robot. The developed measurement system consists of five digital probes. The measurement values from the digital probes are transformed into position and orientation of the end-effector with consideration of measurement system kinematics. Calibration procedure is applied to the probe system and accuracy of the system is measured. After the calibration, the positional accuracy is observed as 0.025mm, and the orientational accuracy is 0.075°, respectively. By using the developed measurement system, we present an experimental result for controller gain tuning about a welding robot. We used Taguchi method to find optimal gain set and succeeded to suppress the fluctuation of the end-effector. The fluctuation with high frequency can be reduced by 54% after gain tuning.

Manuscript received: July 27, 2009 / Accepted: March 18, 2010

NOMENCLATURE

{F} : Fixed frame (world coordinate)
{M} : Moving frame (local coordinate)
{T} : Tool frame
${}^{**}_{*}T$: Transformation matrix from {*} frame to{**} frame
$P_{\{F\}}$: a point in the fixed frame, {F}

1. Introduction

A measurement system is one of the essential elements in the utilization of an industrial robot. We can evaluate the accuracy and repeatability of a robot by measuring the position and orientation of the robot's end-effector with the measurement system. Moreover, the measured data can be used to conduct the kinematic calibration and controller gain tuning.

For measuring the end-effector of industrial robots, many pose measurement systems have been proposed. Huang Jin et al. proposed the robot scanning system with an external axle.[1] Corbel et al. designed a 6-d.o.f parallel measurement mechanism integrated in a parallel 3-d.o.f machine-tool.[2] Lightcap and Weihua measured the poses of a tooling ball, which was attached to an end-effector.[3,4] They used a coordinate measuring machine (CMM) and an LVDT as measurement devices. Di Giacomo and Fabricio developed a multi-probe measurement system and used error separation methods with redundant data.[5,6] Alberto et al. measured the poses of a robot by matching the pin of the end-effector to a hole on a dime.[7] Borm proposed calibration device with a touch sensing device and a calibration jig. This device could find the poses of the end-effector.[8] Recently, vision measurement systems have been used.[9-12] A vision measurement system consists of a camera, a target and a laser sensor. It is useful for measuring the pose of the end-effector of a robot when the robot is operating. Moreover, vision system is convenient to set up.

When the measurement process has to be done at an industrial site such as in the shipbuilding industry or automotive factory, the measurement system should be established with more thoughtful design consideration. At an industrial site, many sources of sensing noise may prevent accurate measurement. The noise sources can include dust, chemical vapors, oil, air contamination, and ambient

temperature change, all of which usually cannot be eliminated. For example, at shipbuilding sites, a measurement system with vision technology would be influenced by electrical noise from welding processes. Moreover, welding fume and limited setup space for the camera system may interfere with accurate pose measurement of the robots.

In this paper, we present an on-site measurement system, which can measure the position and orientation of the end-effector of a welding robot. As shown in Fig. 1, we design the measurement device is easily mounted on the end-effector of the welding robot instead of a welding torch. The developed measurement device can be used in narrow area such as in the shipbuilding industry. For the on-site compatibility, the measurement system is developed with simple distance measuring sensors.

We also show the vibration suppression procedure by tuning controller gains in the servomotor. The developed measurement system can measure the position and orientation as well as the trajectory of the end-effector during operation. By measuring the pose data for the welding robot continuously, the measurement system can obtain trajectory profile for the welding pathways. The measurement system can be applied to tune controller gains with the measured trajectory.

The remainder of this paper is organized as follows. Section 2 presents the pose measurement system for a welding robot. The structure and characteristics of the six-axis robot used in this paper are described in Section 3. The controller gain tuning of the welding robot are discussed in Section 4. Finally, conclusions are given in Section 5.

2. Measurement system

2.1 Measurement device

The on-site measurement systems for a welding robot require several design criteria such as easy installation, structural robustness, convenient use, small size and light weight. If the working direction of the welding robot is set in the x-axis as shown in Fig. 1, the quality of the welding process in the x-direction is influenced by the positional accuracy of the end-effector along the z-axis and y-axis, and by the orientation of the end-effector. Besides, the positional accuracy of a welding robot is required within 0.5mm for the welding quality. From these requirements, we developed a 5-DOF parallel measurement device, as shown in Fig. 2 and a measured artifact. This setup offered many advantages such as simplicity of structural mechanism, ease of analysis, easy applicability on the spot, low expense and a more reliable result.

The measurement system includes the measurement device and the measured artifact. The measurement device consists of the sensor fixture and five digital probes. The sensor fixture, whose function is to fix five digital probes, cut by a laser cutter for measurement precision and has a design tolerance within 0.01mm. We used five digital probes and five AD converters, which were manufactured by Solartron Metrology co., Ltd. The available maximum stroke of the digital probe was 20mm and the resolution of the probe was 1.22μm. The repeatability of the digital probe were suggested by the manufacturer, which were less than 1.22μm. The digital probe is strong against noises because the probe transmits the data after transforming measured values digitally. The overall size and weight of the measurement device with the five probes were 212mm(w)×210mm(h)×35mm(d) and within 1kg, respectively, as shown in Fig. 2. The size of measuring space is 14mm×14mm along the z-axis and y-axis.

A measured artifact is designed with consideration of the workspace of the welding robot. The working path of the welding robot is U-type, whose size is 800mm(w)×600mm(h). The measured artifact consists of three steel bars. The cross section of a steel bar is rectangular, as shown in Fig. 2. All of five probes always should contact the measured fixture during measuring the end-effector.

2.2 Kinematic analysis of the measurement system

The measurement device is a set of sensors, which are installed parallel to each other. Parallel mechanisms suffer the problems of relatively small useful workspace and complex forward kinematics.[13] In this paper, we solved kinematic analysis of 5-DOF parallel mechanism with geometrical characteristic of the measured artifact. Fig. 3 shows the schematic of the measurement device. In this figure, {F} is a coordinate located in the measured fixture. {T} is a coordinate located on the end-effector of the robot and {M} is a coordinate located in the measurement device. P_i (i=1, 2, 3, 4, 5) are the points of intersection between the digital probes and measured artifact in moving coordinate, {M}. P_i' are the points of connection of the digital probes into the sensor fixture. We can find the geometrical configuration of the measured artifact with relations of P_i and obtain transformation matrix between three frames.

2.2.1 Forward kinematics

The forward kinematics of the measurement system represents the position and orientation of the end-effector for sensor values, L_i (i=1, 2, 3, 4, 5). This paper deals with the y and z values, which indicate the position of the end-effector. The x value will be treated with the linear encoder in future work. P_i can be represented by the values of L_i in the moving frame, {M}. A z-direction vector of the fixed frame can be calculated with P_1, P_2 and P_3 in the moving frame, as shown in Eq. (1). There is the equation of the perpendicular plane, which means the upper surface of the measured artifact.

$$\hat{z}^T = \frac{\overrightarrow{P_2P_3} \times \overrightarrow{P_2P_1}}{\left|\overrightarrow{P_2P_3} \times \overrightarrow{P_2P_1}\right|} = [a_z, b_z, c_z], \quad a_z x + b_z y + c_z z = d_z \tag{1}$$

A y-direction vector of the fixed frame can be calculated with P_4, P_5 and the z-direction vector (2). An x-direction vector is the outer product of the z-vector and the y-vector (3).

$$\hat{y} = d_y A^{-1} \begin{bmatrix} \hat{0} \\ 1 \\ 1 \end{bmatrix} \text{ where, } A = \begin{bmatrix} \hat{z}^T \\ P_4^T \\ P_5^T \end{bmatrix}, \text{ (3x3 matrix)} \tag{2}$$

$$\hat{x} = \hat{y} \times \hat{z} \tag{3}$$

Table 1 Kinematic parameters of measurement system

Variable	Values	Variable	Values
L_1~L_5	Digital probe	U_C	9mm
P_1~P_5	End points of probe	D	135mm
P_1`~$P_5$`	Start points of probe	K	7.5mm
U	135mm	θ	45°

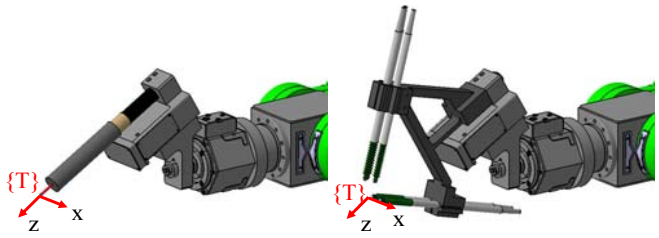

Fig. 1 Solid model of installation of measurement device instead of a welding torch at the end-effector of a welding robot

The rotation matrix from {F} to {M} is represented with x, y and z direction vectors, as shown in Eq. (4).

$$ {}^{M}_{F}R = {}^{F}_{M}R^{-1} \quad \text{where,} \quad {}^{F}_{M}R = [\hat{x} \quad \hat{y} \quad \hat{z}] \tag{4}$$

The orientation (α, β, γ) of the end-effector is obtained from the rotation matrix of (4).

$$\begin{aligned} \alpha &= \tan^{-1}(r_{21}/r_{11}), \\ \beta &= \tan^{-1}(-r_{31}/\sqrt{r_{11}^2 + r_{21}^2}), (\because -90 \le \beta \le 90), \\ \gamma &= \tan^{-1}(r_{32}, r_{33}) \end{aligned} \tag{5}$$

Where, r_{ij} is a component of the rotation matrix, ${}^{M}_{F}R$

The values of y and z are calculated by using the distance from the perpendicular/horizontal plane to the end point, P_t in the moving frame.

$$y = W - \frac{|a_y x_t + b_y y_t + c_y z_t - d_y|}{\sqrt{a_y^2 + b_y^2 + c_y^2}} \tag{6}$$

$$z = H - \frac{|a_z x_t + b_z y_t + c_z z_t - d_z|}{\sqrt{a_z^2 + b_z^2 + c_z^2}} \tag{7}$$

Where, $P_t = \begin{bmatrix} x_t \\ y_t \\ z_t \end{bmatrix}$

2.2.2 Inverse kinematics

Inverse kinematics is used to calculate the values of sensors from the position and orientation of the end-effector. The distances between P_i and P_i' are the same as the values of L_i in Fig. 3. The point, P_i' can be represented in the moving frame and transformed to ${}^{\{F\}}P_i'$ in the fixed frame by multiplying the transformation matrix from {F} to {M}. The transformation matrices are obtained from Eq. (8), (9) and (10).

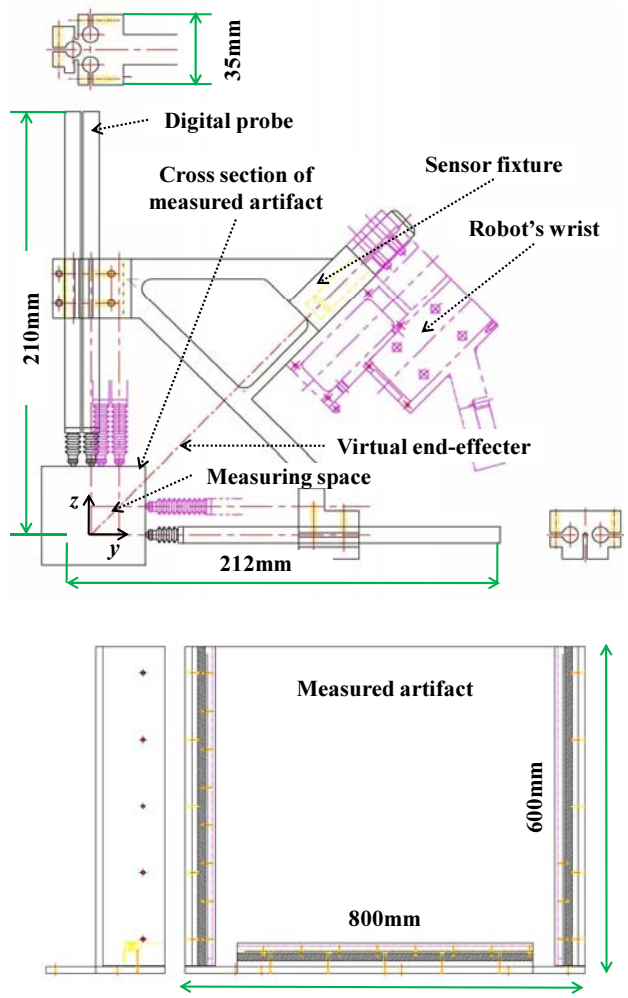

Fig. 2 Drawing of measurement system

Table 2 The accuracy and deviation at the end-effector of the measurement system after the calibration

	y	z	α	β	γ
Unit	(mm)		(degree)		
Measured accuracy	0.024	0.019	0.066	0.071	0.043

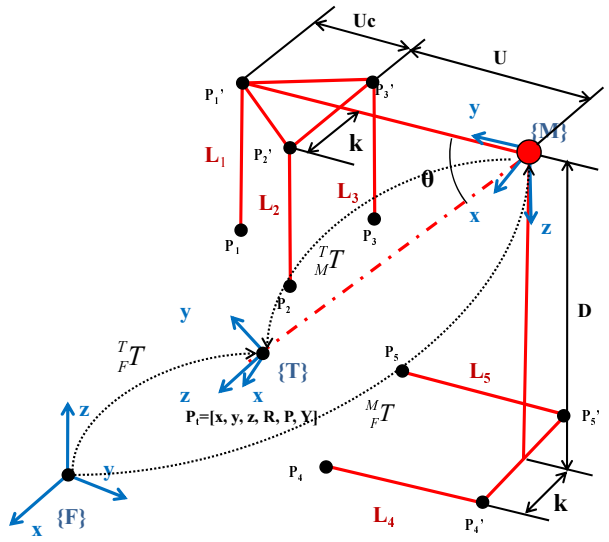

Fig. 3 Schematic of measurement system

$$ {}^{T}_{F}T = \begin{bmatrix} {}^{T}_{F}R & {}^{T}_{F}P \\ 0 & 1 \end{bmatrix}, (\because {}^{T}_{F}R = R(z,\alpha)R(y,\beta)R(x,\gamma),\ {}^{T}_{F}P = [x,y,z]^{T} \quad (8) $$

$$ {}^{T}_{M}T = \begin{bmatrix} {}^{T}_{M}R & {}^{T}_{M}P \\ 0 & 1 \end{bmatrix}, (\because {}^{T}_{M}R = R(x,45^{\circ}),\ {}^{T}_{F}P = [0,135,135]^{T} \quad (9) $$

$$ {}^{M}_{F}T = {}^{T}_{F}T({}^{T}_{M}T)^{-1} \quad (10) $$

We defined V_i as a directional vector of L_i. The V_i can be transformed to $V_{i\{F\}}$ like $P_i`_{\{F\}}$. $P_{i\{F\}}$ is the point of intersection of a plane ($z = H$ or $y = W$) and a line, which is expressed by $V_{i\{F\}}$ and $P_i`_{\{F\}}$. Accordingly, L_i can be obtained from Eq. (11)

$$ Li = \left| P_{i_{\{F\}}} - P_{i_{\{F\}}} \right| \ (\because i = 1,2,3,4,5) \quad (11) $$

2.3 Accuracy and repeatability of the measurement system

We used CMM(Coordinate Measuring Machine) in order to assess the accuracy of the measurement system as shown in Fig. 4. The twelve points were measured and the accuracy was assessed from differences between the data from the measurement system and the data from CMM. Before kinematic calibration, the positional error in y axis and z axis are 0.192mm and 0.080mm, (which is root-mean-square value for positional error), respectively. The rotational error in x, y, and z axis, (α, β and γ) are 0.348°, 0.549° and 0.430°, respectively.

We built an error model with fifteen kinematic parameters for the measurement system. The error of the kinematic parameters were calibrated with measured position by CMM. With the error modeling we could obtain the accuracy of the measurement system. After the calibration, the accuracy in the y and z direction are measured as 0.024mm and 0.019mm, respectively. The accuracy of α, β and γ orientation are 0.066°, 0.071° and 0.043°, respectively. Fig. 5 represents the result of kinematic calibration in the y direction and α orientation.

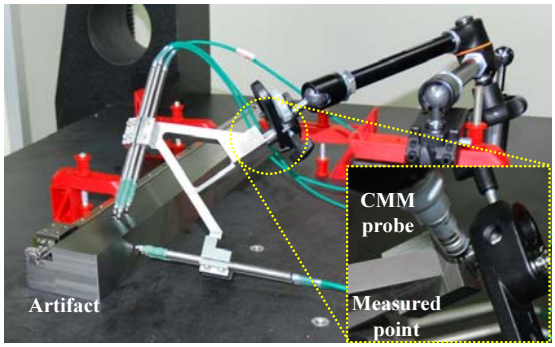

Fig. 4 Measurement set up of the measurement system with CMM

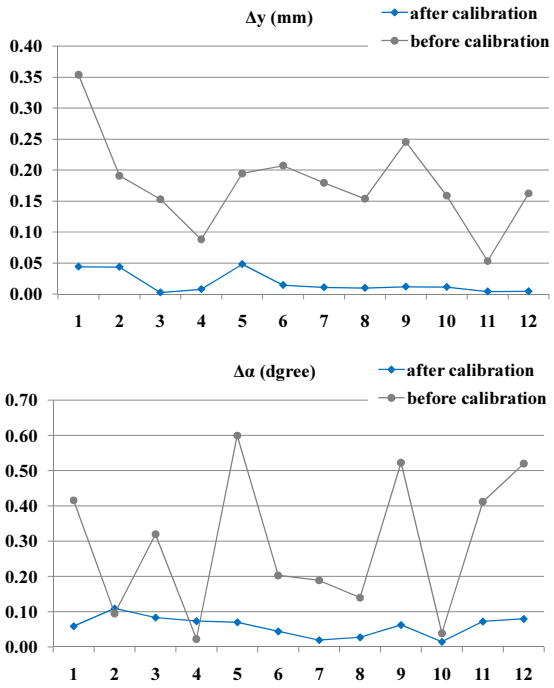

Fig. 5 The result graph of calibration

3. The experimental set-up

The measurement system is applied to tune the controller gains of the six-axis manipulator of the welding robot shown in Fig. 6. The welding robot has 3-Revolute joints and 3-Prismatic joints. The size of the welding robot is 1137 (w) × 1537 (h) × 1376 (d). The Denavit-Hartenberg parameter method is used to carry out the kinematic analysis of the robot. Also, the manipulator is driven by the AC servo motor, and the motions are limited by micro limit switches.[14]

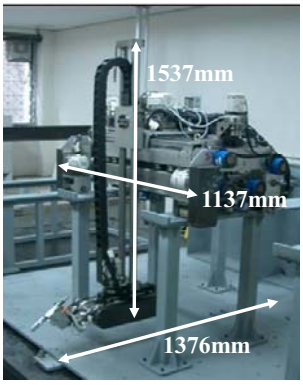

Fig. 6 Photo of manipulator and mobile platform

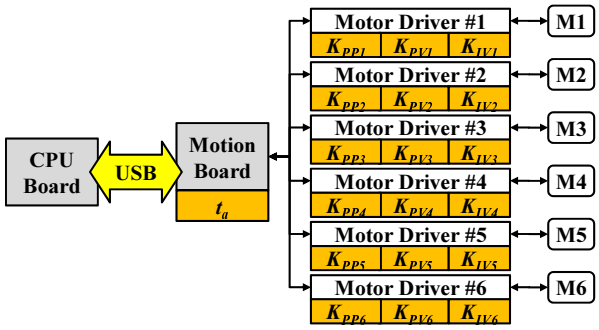

K_{PP} : Proportional gain for position control
K_{PV} : Proportional gain for velocity control
K_{IV} : Integral gain for velocity control
t_a : Acceleration/Deceleration time

Fig. 7 Configuration of the control system of the welding robot

Fig. 7 shows the configuration of the control system of the welding robot. The main controller of the manipulator consists of a CPU board, a motion controller that can perform linear interpolation for all of six axes, and six AC servo motor drivers. The CPU board generates the motion path between the start points and end points and calculates the angles of all the joints and gives motion signals to the motion controller through USB communication. The motion controller receives commands from the CPU board, and then controls the six AC servo motor drivers.

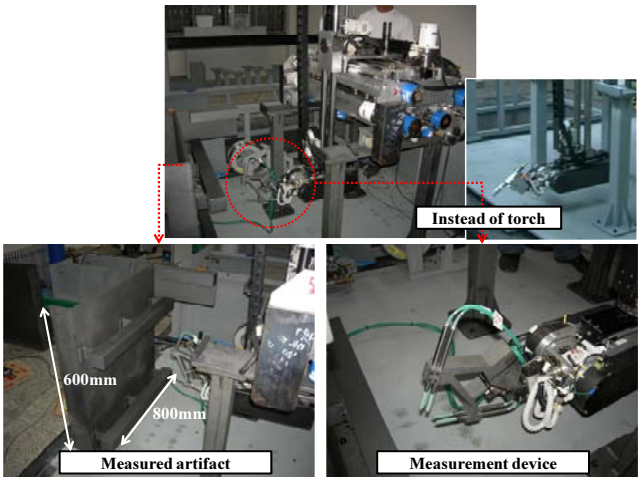

Fig. 8 General view of the experimental setup

The welding manipulator executes a horizontal and vertical motion. The manipulator moves linearly in horizontal motion but moves weave-like in the vertical motion. For measuring these motions, the measurement device is mounted in the wrist of the welding robot instead of the welding torch, as shown in Fig. 8. And then the welding robot moves during five probes are in contact with the measured artifact.

4. Gain tuning of controller parameters

By using the suggested system and the Taguchi method, the controller gains tuning for the welding robot was executed in Cartesian space.

In fact, it is easy to tune control gains in a joint space. Also, many methods have been used to tune controller gains in a joint space.[15-17] However, the gains have to be re-tuned for operating multi-axis simultaneously because tuned gains in a joint space are difficult to be adopted in a Cartesian space.[12] Moreover in the case of MIMO, since there are many number of gains, the overall tuning of gains can be more complex.[18]

Taguchi method can determine controller gains without using a mathematical model to control the system. Also, the number of experiments for tuning controller gains can be reduced by using an orthogonal array.[19]

The welding robot, which was used in the experimental set-up described in this study, had nineteen controller gains, as shown in Fig. 7. As tuning these gains, we can suppress vibrations of the end-effector.

4.1 Taguchi method

The 'Design of Experiment' using the Taguchi method is briefly outlined below.[20]

Identifying the objectives: In the first step of the Taguchi method, identifying a specific objective is important. In the experiment of this paper, a vibration is generated when the end-effector of the manipulator has a change of direction in a vertical motion with weaving. Therefore, the objective is a robust tuning of controller gains for suppressing the vibration of the end-effector.

Determining the quality characteristic: The quality characteristic of this study is the maximum magnitude among frequencies in high frequency area more than 2.4Hz, and it is smaller-the-better problem.

Selecting the controllable factors and noise factors: Controller gains are used as the controllable factors. The operating velocity of the manipulator is selected as the noise factor. The number of levels for controllable factors is two in sensitive analysis and three in optimization experiment and for operated velocity is two.

Selecting an orthogonal array: Nineteen controllable factors were selected. In this case, $L_9(3^4)$ is used as the orthogonal array with obtained controllable factors from the sensitivity analysis since there is no suitable orthogonal array for nineteen controllable factors.

Conducting the experiment and analysis: The experimental result with the controllable factors and noise factors can be converted into the representative signal-to-noise ratio (S/N ratio, η). We can adapt the S/N ratio as the barometer of the ability of the system to perform well in relation to the effect of noise. We can also determine the control factor settings that can produce the best performance in a process or product while minimizing the defect of these influences we cannot control. In this experiment, η is expressed as

$$\eta_i = -10\log_{10}\left(\frac{1}{4}\sum_{j=1}^{4} y_{ij}^{\,2}\right) \tag{12}$$

where y_{ij} for experiment number i = 1, 2, ..., 9 and levels of noise factor j = 1, 2 is the index of the aggregate maximum frequency.

4.2. Experiments

The experiment of this paper considers only vertical motions with respect to vibration. The welding robot has a weaving motion during vertical motion. The weaving motion is to move in zigzags. Because of the weaving motion, there is predominant vibration during vertical motion but not during horizontal motion.

Fig. 9 represents the commanded motion in the x/y plane and the measured trajectory of the end-effector in the x-dir and y-dir during vertical motion. Although the command signal is sine wave at a change of direction, vibrations of less than 0.5mm amplitude are generated in measured trajectory.

The command value and the measured value are transformed in the frequency domain using FFT for vibration analysis. As shown in Fig. 10, when a vibration is generated, there are the magnitudes of

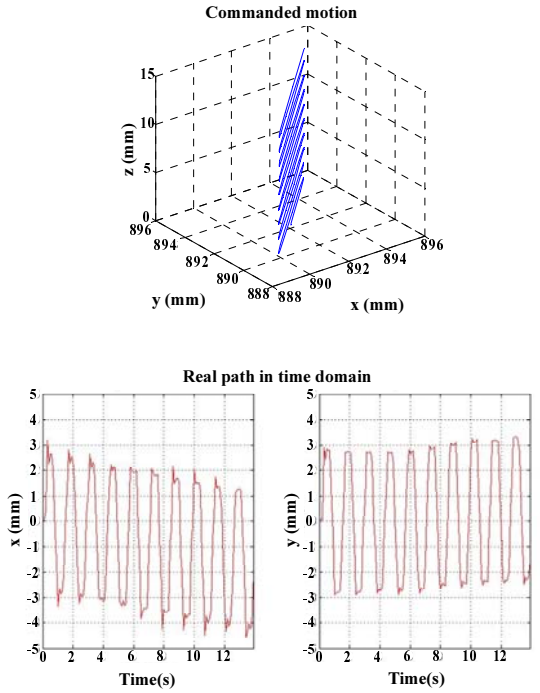

Fig. 9 The commanded motion and the measured trajectory in the x and y directions

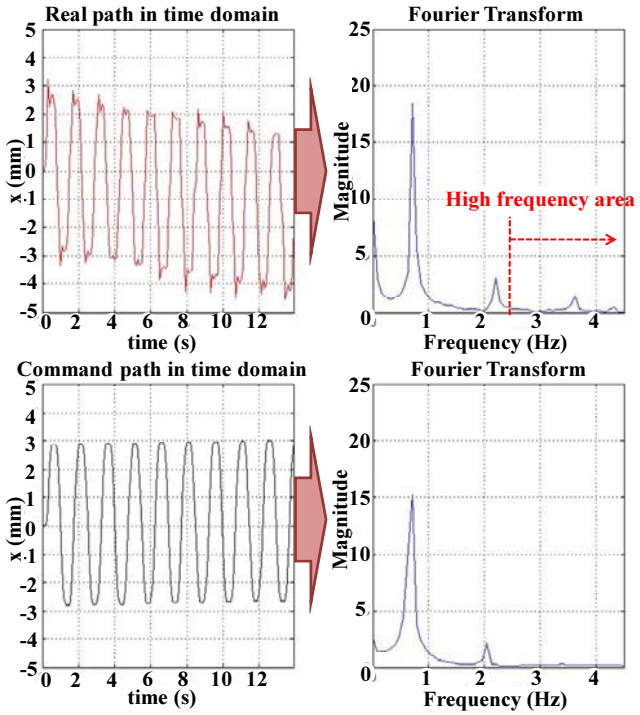

Fig. 10 Fast Fourier Transform of a trajectory at the end-effector

the high frequency in a frequency domain. We take the maximum signal in the high frequency a quality characteristic. The controllable factors which minimize the S/N ratio for the maximum signal can be obtained in this experiment. Additionally, there is a significant drift(1mm) in Fig. 10. The drift could be caused by backlash, kinematic errors of the welding robot. In this study, however, we focused on the vibrational suppression of the target robot at a change of direction only. Only motor gains could influence the vibration of the end-effector, and other factors could be ignored for the vibration suppression.

There are 19 gains related to the vibration of the end-effector. If the test is carried out with all controllable factors, a study involving 19 factors at three levels each would require 3^{19} = 1,162,261,467 experiments.

The number of experiments can be reduced remarkably if we use an orthogonal array based on Taguchi method. We used the orthogonal array as well as the sensitivity analysis for the application of the orthogonal array.

The experiment using the Taguchi method for gain tuning has three stages. The first stage is sensitivity analysis for selection of the controllable factors which are more sensitive than other parameters to vibration. From the sensitivity analysis, we could obtain four controllable factors, K_{PP1} of servomotor M_1, K_{PP3}, K_{IV3} of servomotor M_3 and acceleration/deceleration time, t_a. Then the four controllable factors are optimized in the first and second optimal experiments which are the second stage and third stage, respectively. The fifteen factors except the selected four controllable factors can use the initial values because the controller manufacturer preset the initial gains to their optimal values. Two optimization experiments have the orthogonal array, $L_9(3^4)$, and the velocity of the end-effector, f, as noise factor.

Table 3 Physical values of three levels and noise factors at the second optimization experiment

Group	Symbol	Level 1	Level 2	Level3
Controllable factors (controller gains)	K_{P1}	650	**800**	950
	K_{P3}	2350	2400	**2450**
	K_{I3}	57.5	60	**62.5**
	t_a	0.194(s)	0.2(s)	**0.206**(s)
Noise factor	f	10mm/s	20mm/s	

Table 4 experiment results based on orthogonal array L9(34) at the second optimization experiment

	Controller gains				Maximum frequency index (y) At different levels of noise factor				S/N ratio
	K_{P1}	K_{P3}	K_{I3}	t_a	f_L(x)	f_L(y)	f_H(x)	f_H(y)	η(dB)
1	1	1	1	1	1.031	0.658	1.190	0.788	0.540
2	1	2	2	2	0.854	0.758	1.477	0.671	0.070
3	1	3	3	3	0.967	0.495	0.886	0.821	1.805
4	2	1	2	3	0.676	0.608	1.241	1.003	0.740
5	2	2	3	1	0.840	0.678	1.119	0.794	1.180
6	2	3	1	2	0.905	0.618	1.112	0.978	0.713
7	3	1	3	2	0.861	0.571	1.994	1.004	-1.798
8	3	2	1	3	0.730	0.622	1.516	0.987	-0.205
9	3	3	2	1	0.885	0.572	1.894	0.545	-0.964

The physical values of each level at the first optimization experiment are determined around the corresponding initial value, which had been individually tuned by controller manufacturer. And then, the physical values at the second optimization experiment are determined from the obtained values at the first optimization experiment. Table 3 represents the physical values of the optimization experiment. As shown in Table 4, the experiment number is from 1 to 9 and two experiments according to the noise

factor levels were executed for each experiment number. Therefore, a total of 9×2=18 experiments were performed in one optimization experiment. And the average S/N ratio for each level of the controllable factors K_{PP1}, K_{PP3}, K_{IV3} and t_a can be calculated by using Eq. (12) and are shown in Fig. 11. The slopes between the points plotted can be compared by plotting the average response value for each factor level. The bold text in the Table 3 is the result of the second optimization experiment.

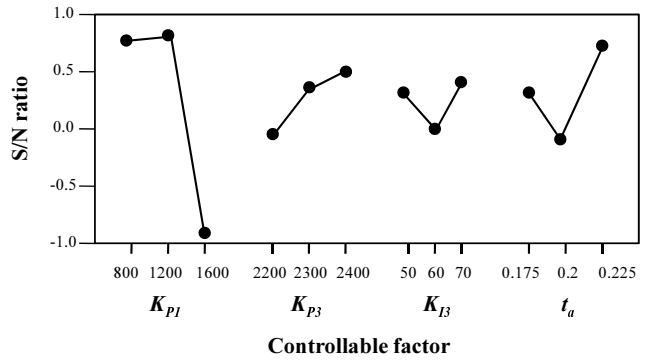

Fig. 11 Response graph obtained at the second optimization experiment for four controllable factors

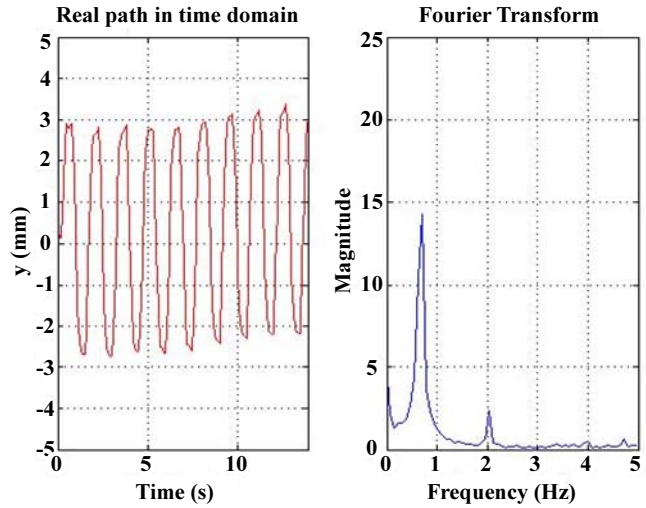

Fig. 12 Trajectory and FFT in the y-axis after gain tuning using the Taguchi method

The second optimization experiment was carried out in the same manner as the first optimization experiment. Fig. 12 represents the trajectory of the end-effector and the FFT after gain tuning of the welding robot. The magnitude of high frequency in the frequency domain was reduced by 54%.

5. Conclusions

A new measurement system was developed to measure the position and orientation of the end-effector of a 6-axis welding robot. The measurement device was the 5-DOF parallel mechanism and consists of five digital probes. For measuring the poses of the end-effector, the measurement device was mounted in the wrist of the welding robot instead of the welding torch.

There was the assessment of the system accuracy using kinematic calibration with CMM. The positional accuracy of the measurement system was less than 0.024mm and the rotational accuracy is 0.071°.

The measurement system is applied to tune the controller gains of the six-axis manipulator of the welding robot. The welding manipulator, which was used in the experimental set-up described in this study, had nineteen controller gains.

We suppressed the vibration of the end-effector of the welding manipulator by tuning controller gains in the servomotor based on Taguchi method. The optimal gains were obtained through the two optimization experiments. The maximum magnitude of the frequency in the high frequency area was reduced by 54%.

ACKNOWLEDGEMENT

This paper was supported by Daewoo Shipbuilding & Marine Engineering, by 2009 Kookmin research program, and by the Seoul R&BD Program (Grant No. 10583).

REFERENCES

1. Jin, H., Zi, M., Yang, W. and Shuanghe, Y., "Industry robot and external axle calibration using particle swarm optimization," Proceedings of the 6th IEEE International Conference on Industrial Informatics, pp. 458-462, 2008.

2. Corbel, D., Company, O. and Pierrot, F., "Optimal design of a 6-d.o.f. parallel measurement mechanism integrated in a parallel 3-d.o.f. machine-tool," Proceedings of 2008 IEEE/RSJ International Conference on Intelligent Robots and Systems (IROS'08), pp. 1970-1976, 2008.

3. Lightcap, C., Hammer, S., Schmitz, T. and Banks, S., "Improved positioning accuracy of the PA10-6CE robot with geometric and flexibility calibration," IEEE Transactions on Robotics, Vol. 24, No. 2, pp. 452-456, 2008.

4. Xu, W. and Mills, J. K., "A new approach to the position and orientation calibration of robots," Proceedings of the 1999 IEEE International Symposium on Assembly and Task planning, pp. 268-273, 1999.

5. Di Giacomo, B., Tsunaki, R. H. and Paziani, F. T., "Robot-based dedicated measuring system with data redundancy for profile inspection," Proceedings of 2005 IEEE/RSJ International Conference on Intelligent Robots and Systems (IROS'05), pp. 1392-1395, 2005.

6. Paziani, F. T., Di Giacomo, B. and Tsunaki, R. H., "Robot measuring form errors," Robotics and Computer-Integrated Manufacturing, Vol. 25, No. 1, pp. 168-177, 2009.

7. Omodei, A., Legnani, G. and adamini, R., "Calibration of a

measuring robot: Experimental results on a 5 DOF structure," Journal of Robotic Systems, Vol. 18, No. 5, pp. 237-250, 2001.

8. Borm, J. H., "An efficient calibration procedure of arc welding robots for offline programming application," Journal of the KSPE, Vol. 13, No. 1, pp. 131-142, 1996.
9. Lei, S., Jingtai, L., Weiwei, S. and Xingbo, H., "Geometry-based robot calibration method," Proceedings of 2004 IEEE International Conference on Robotics and Automation (ICRA'04), Vol. 2, pp. 1907-1912, 2004.
10. Watanabe, A., Sakakibara, S., Ban, K., Yamada, M. and Shen, G., "A kinematic calibration method for industrial robot using autonomous visual measurement," Annals of the CIRP, Vol. 55, No. 1, pp. 1-6, 2006.
11. Renaud, P., Andreff, N., Lavest, J.-M. and Dhome, M., "Simplifying the kinematic calibration of parallel mechanisms using vision-based metrology," IEEE Transactions on Robotics, Vol. 22, No. 1, pp. 12-22, 2006.
12. Cheah, C. C., Hirano, M., Kawamura, S. and Arimoto, S., "Approximate Jacobian control for robots with uncertain kinematics and dynamics," IEEE Transactions on Robotics and Automation, Vol. 19, No. 4, pp. 692-702, 2003.
13. Liu, X.-J., Wang, J. and Kim, J., "Determination of the link lengths for a spatial 3-DOF parallel manipulator," Journal of Mechanical Design, Vol. 128, No. 2, pp. 365-373, 2006.
14. Lee, D., Lee, S., Ku, N., Lim, C., Lee, K., Kim, T. and Kim, J., "Development and Application of a Novel Rail Runner Mechanism for Double Hull Structures of Ships," Proceedings of 2008 IEEE International Conference on Robotics and Automation (ICRA'08), pp. 3985-3991, 2008.
15. Mohamed, Z., Martins, J. M., Tokhi, M. O., Sa da Costa, J. and Botto, M. A., "Vibration control of a very flexible manipulator system," Control Engineering Practice, Vol. 13, No. 3, pp. 267-277, 2005.
16. Wang, C. C. and Tomizuka, M., "Sensor-based Controller Tuning of Indirect Drive Trains," Proceedings of the 10th IEEE International Workshop on Advanced Motion Control, pp. 188-193, 2008.
17. Chang, T. N., Kwadzogah, R. and Caudill, R. J., "Vibration Control of Linear Robots Using a Piezoelectric Actuator," IEEE/ASME Transactions on Mechatronics, Vol. 8, No. 4, pp. 439-445, 2003.
18. Lee, J. W., "A systematic gain tuning of PID controller based on the concept of time delay control," Int. J. Precis. Eng. Manuf., Vol. 9, No. 4, pp. 39-44, 2008.
19. Lee, K. and Kim, J., "Controller gain tuning of a simultaneous multi-axis PID control system using the Taguchi method," Control Engineering Practice, Vol. 8, No. 8, pp. 949-958, 2000.
20. Peace, G. S., "Taguchi Methods: A hands-on approach to quality engineering," Addison-Wesley, 1993.